# Short-term plasticity of 7T BOLD ocular dominance and spatial frequency representation in adult human primary visual cortex

Paola Binda#[1], Jan W. Kurzawski#[2], Claudia Lunghi[1,3], Laura Biagi[2], Michela Tosetti[2,4], Maria Concetta Morrone*[1,2]

*[1]University of Pisa, Italy; [2]IRCCS Stella Maris, Calambrone, Pisa, Italy; [3]Laboratoire des systèmes perceptifs, Département d'études cognitives, École normale supérieure, PSL Research University, CNRS, 75005 Paris, France; [4]IMAGO Center, Pisa, Italy.*

# co-first authors

* Lead contact and corresponding author
Maria Concetta Morrone
*University of Pisa,*
*Department of Translational Research and New Technologies in Medicine and Surgery*
Via San Zeno 31, 56123 Pisa (PI), Italy
concetta@in.cnr.it

## Abstract

Primary visual cortex is considered to be resilient to plastic changes in adults – particularly ocular dominance, which appears to be hard-wired after the end of the critical period. We show that short-term (2h) monocular deprivation unexpectedly shifts ocular dominance in favor of the deprived eye: contrary to common belief. The plastic response of V1 (measured with 7T fMRI) consists of a homeostatic increase of the deprived-eye BOLD response, a shift of V1 ocular dominance and a decrease of spatial frequency selectivity for the deprived eye. These effects reliably predict the robust perceptual changes induced by deprivation at the individual participant level. Our results indicate that primary visual cortex retains a high potential for homeostatic plasticity in the human adult.

## Significance statement

Plasticity, the brain reorganization in response to deprivation, is maximum during development but decreases in adulthood, particularly in primary sensory areas. Here we show, for the first time, that short-term sensory deprivation in human adults transiently changes key functional properties of primary visual cortex. Our participants applied a translucent patch on one eye for 2h, after which two key properties of V1 (measured with ultra-high field fMRI) were systematically changed:

ocular dominance and acuity. Our study is the first that directly shows eye-specific and stimulus-specific plastic modulation in V1. Crucially, these changes correlate tightly with the individual perceptual effect – yielding congruent and reliable biomarkers of an individual's residual cortical plasticity, the first step towards exploiting this potential in disease.

## Introduction

To interact efficiently with the world, our brain needs to fine-tune its structure and function, adapting to a continuously changing external environment. This key property of the brain, called *neuroplasticity* (1), is maximal early in life, within the so called *critical period* (2-5), but it is thought to decline dramatically during adulthood, especially at the level of the primary sensory cortices. During development, plastic cortical response to abnormal visual experience is so strong that occluding one eye for a few days induces a dramatic and permanent shift in ocular dominance (the amount of V1 neurons responding to each eye) in favor of the open eye (2-6), while the deprived eye becomes functionally blind or very weak, a phenomenon known as amblyopia (2, 6-8). After the closure of the critical period, V1 is thought to become fundamentally hard-wired: much longer monocular deprivation time (several weeks/months) is necessary to observe only a modest shift in ocular dominance in animal models (9).

In humans, very little is known about the neural mechanisms underlying neuroplasticity of the adult visual cortex – which, like in the animal model, appears to be more characterized by stability of its processes and representations rather than their plasticity (10-12). Visual plasticity in adult humans have been mainly studied with two approaches: classically with perceptual learning and more recently with short term deprivation. Perceptual learning requires long training sessions repeated over several days in combination with positive reward (13-18). In spite of extensive research, it is still debated whether perceptual learning fine-tunes the neuronal responses at level of primary visual cortex or whether the effect primarily lies in associative cortices (18-24), which usually retain a higher level of plasticity in adulthood. More recently, psychophysical studies have revealed a form of adult plasticity after short-term deprivation, probably associated with an alteration of primary visual cortex processing, where deprivation paradoxically leads to enhanced sensitivity. For example, selective deprivation of one cardinal orientation over few hours leads to paradoxically enhanced sensitivity to the deprived orientation (25). Similarly, short-term monocular deprivation leads to a transient boost of the deprived eye responses (26-32).

The boost of the deprived eye after short-term monocular deprivation is consistent with homeostatic plasticity, an initial compensatory reaction of the visual system to deprivation aimed at maintaining the average cortical activity constant despite the impoverished incoming visual input(33). Homeostatic plasticity was first reported in animal models, where – unlike the human data – it was studied during the developmental critical period and observed after many days of monocular deprivation (33-36). Homeostatic plasticity has been associated with a dynamic synaptic scaling and changes in the balance between excitation and inhibition(37), and GABA may be a key player. Interestingly, short-term plasticity in adult humans is accompanied by a decrease in resting GABA concentration in the occipital visual cortex, observed after deprivation in human adults by MR-spectroscopy (26). This is also in line with the decrease of inhibition after full visual deprivation (blindfolding), measured by TMS, pharmacological manipulations and BOLD (38-41). A decrease of GABA should affect not only overall neuronal excitability, but also neuronal selectivity, as both orientation and spatial frequency selectivity are mediated by GABAergic intra-cortical inhibitory circuitry (reviewed in42). Here we measured 7T BOLD responses in adult humans before and after 2 hours of Monocular Deprivation (MD). With a newly developed technique, we were able to demonstrate a change of ocular dominance and of neuronal selectivity of primary visual cortex during homeostatic plasticity. Our fMRI and psychophysics provide reliable and congruent biomarkers of the residual cortical plasticity in each individual adult participant.

## Results

### Monocular deprivation boosts V1 responses to the deprived eye and shifts BOLD ocular dominance

To investigate the visual modulation of BOLD signal by short term deprivation, we performed ultra-high field (UHF, 7T) fMRI during the presentation of high contrast dynamic bandpass visual stimuli, delivered separately to the two eyes, before and after 2 h of monocular contrast deprivation (see schematic diagram in Fig. 1A).

We first analyzed responses to stimuli with the highest spatial frequency (peak 2.7 cycles per degree, cpd) – given that prior evidence showed robust psychophysical effects of monocular deprivation in this spatial frequency range (26, 27, 29, 43). The reliability and high signal-to-noise ratio of our system allow us to obtain significant activations of all the main visual areas (Fig. 1B), and particularly of V1/V2, with only two blocks of stimulation (Fig. 1B). In addition, the variability of the response across participants is very small, as indicated by the small error bars of the event-related average (V1 BOLD modulation synchronized to stimulus onset) in Fig. 1C (each point is acquired only twice per participant).

This strong and reliable response enabled us to measure the short-lived effect of monocular deprivation, by comparing response amplitudes for stimuli in the two eyes before and after deprivation. Fig. 1D shows that the V1 response to the stimuli presented in the left and right eye is nearly equal before deprivation ("PRE"). However, after deprivation ("POST"), the response in the two eye changes in opposite directions, with a boost of the BOLD response (measured as GLM Beta values) of the deprived eye and a suppression of the non-deprived eye (see also supplementary Fig. S1). This was formally tested with a two-way repeated measure ANOVA, entered with the median BOLD responses across all vertices in the left and right V1 region, for the four conditions and each participant (Fig. 1D show averages of this values across participants). The result reveals a significant interaction between the factors *time* (PRE, POST deprivation) and *eye* (deprived, non-deprived; interaction term $F(1,17) = 13.35106$, $p = 0.002$). Fig. 1E confirms these findings with an analysis of the aggregate subject data, obtained by pooling all V1 vertices across all subjects. For each vertex, we defined an index of Ocular Dominance, as the difference of BOLD response to the deprived and non-deprived eye. Before deprivation, the Ocular Dominance index is symmetrically distributed around zero, indicating a balanced representation of the two eyes before deprivation (yellow distribution in Fig.1E). After deprivation (black distribution in Fig.1E), the ocular dominance distribution shifts to the right of 0, indicating a preference for the deprived eye (non-parametric Wilcoxon sign-rank test comparing the PRE and POST Ocular Dominance medians, $z = 113.59$, $p < 0.001$). In principle, the boost of responses to the deprived eye seen in Fig. 1D could be produced by enhancing the response of vertices that originally preferred the deprived eye (without shifting ocular dominance) or by changing Ocular Dominance of vertices that originally preferred the non-deprived eye, driving them to prefer the deprived eye after deprivation. The shift of the Ocular Dominance histogram in Fig. 1E is more compatible with the latter case, which would be functionally corresponding to a recruitment of cortical territory for the representation of the deprived eye.

To investigate this further, we monitored the final POST-deprivation Ocular Dominance of individual vertices that, PRE-deprivation, preferred the deprived eye (yellow half distribution in Fig 2A). The majority of vertices continue to prefer the same eye before and after deprivation. The median Ocular Dominance is significantly larger than 0 both PRE and POST (Wilcoxon sign-rank test, $z > 96$, $p < 0.0001$ in both cases) and the correlation between Ocular Dominance indices before and after deprivation is strong and positive (Pearson's $R(29219) = 0.22$ [0.20-0.23], $p < 0.0001$). Note that a completely random reassignment of Ocular Dominance after deprivation would have produced a histogram centered at 0 and no correlation between Ocular Dominance indices PRE- and POST deprivation. This is not consistent with the results of Fig. 2B, which thereby provide

evidence that our estimates of Ocular Dominance before and after deprivation are congruent, even though they were collected in different fMRI sessions separated by 2h. In addition, the distribution of Ocular Dominance after deprivation is well predicted by adding only a small amount of noise to the original half distribution (Gaussian noise with 0.12 standard deviation, black line), suggesting that these vertices were largely unaffected by monocular deprivation. This is also supported by the repeated measure ANOVA of individual subject data (Fig. 2A), revealing a strong main effect of eye ($F(1,17) = 36.92$, $p = 0.00001$): the response to the deprived eye is stronger than the non-deprived eye, both before deprivation (due the selection, $t(17) = -8.935$, $p < 10^{-5}$), and after deprivation ($t(17) = -3.725$, $p = 0.002$), with no effect of time and no *time* × *eye* interaction (all $F(1,17) < 0.2$, $p > 0.5$).

A completely different pattern is observed for the vertices originally preferring the non-deprived (yellow half-distribution in Fig. 2D). Here the distribution of Ocular Dominance clearly shifts after deprivation; the median moves from significantly negative before deprivation (Wilcoxon sign-rank test, $z = -172.17$, $p < 0.0001$) to significantly positive after deprivation (Wilcoxon sign-rank test, $z = 60.35$, $p < 0.0001$), implying a shift of dominance in favor of the deprived eye. Again, this is not consistent with a random reassignment of Ocular Dominance after deprivation, which predicts a distribution centered at 0. Contrary to Fig. 2B, the POST- Ocular Dominance distribution cannot be predicted by injecting Gaussian noise to the PRE- Ocular Dominance distribution (black line, 0.12 standard deviation like for Fig. 2B): for these vertices, there is a shift of Ocular Dominance with short term monocular deprivation. This is confirmed with the repeated measure ANOVA (Fig. 2C), where the *time* × *eye* interaction is significant ($F(1,17) = 36.64$, $p = 0.00001$), implying a different modulation PRE and POST deprivation. In addition and crucially, POST-deprivation BOLD responses to the deprived eye are significantly larger than POST-deprivation responses to the non-deprived eye ($t(17) = -2.426$, $p = 0.027$; whereas, by selection, the opposite is true before deprivation: $t(17) = 10.538$, $p < 10^{-5}$).

In summary, ocular dominance before deprivation defines two similarly sized sub-regions of V1 vertices (43.95 ± 5.66% and 56.05 ± 5.66% of analyzed V1 vertices; 30.92 ± 3.72 % and 41.28 ± 4.51 % of all V1 vertices) with radically different behaviors that are not consistent with an artifact induced by vertex selection. The sub-region that originally represents the deprived eye does not change with deprivation; the sub-region that originally represents the other non-deprived is rearranged with deprivation, as a large portion of vertices turn to prefer the deprived eye.

We used Binocular Rivalry, measured just before the PRE- and POST-deprivation fMRI sessions, to estimate psychophysically the effect of monocular deprivation on perceptual ocular dominance. In line with previous studies (26, 27, 29, 30, 43), short-term monocular contrast deprivation induced a 30% increase of phase duration for the deprived eye (POST to PRE-deprivation ratio: 1.30 ± 0.31) and a 15% decrease of phase duration for the non-deprived eye (ratio: 0.86 ± 0.31), producing a significant *time* × *eye* interaction (Fig. 3A, repeated measure ANOVA on the mean phase durations for each participant, interaction: $F(1,17) = 21.40085$, $p = 0.00024$). We defined a psychophysical index of the deprivation effect ($DI_{psycho}$) by using Eq. 6 in methods section, where the POST to PRE-deprivation ratio of phase durations for the deprived eye, is divided by the same ratio for the non-deprived eye. Values larger than 1 imply a relative increase of the deprived eye phase duration, i.e. the expected effect; a value less than 1 indicates the opposite effect and a value of 1 indicates no change of mean phase duration across eyes. All but two subjects have values larger than 1, indicating a strong effect of deprivation. However, the scatter is large with values ranging from 0.7 to 3, suggesting that susceptibility to visual plasticity varies largely in our pool of participants. Capitalizing on this variability, we tested whether the size of the psychophysical effect correlates with the BOLD effect across participants. Using the same Eq. 6 to compute the deprivation effect on BOLD responses ($DI_{BOLD}$), we observed a strong correlation between the effect of monocular deprivation on psychophysics and BOLD (shown in Fig. 3B). Subjects who showed a strong deprivation effect at psychophysics ($DI_{psycho} > 2$) also showed a strong deprivation effect in BOLD responses ($DI_{BOLD} = 1.82 \pm 0.35$). Given that the psychophysics was measured only for central vision and at 2 cpd stationary grating, whereas BOLD responses were pooled across a large portion on V1 and were elicited using broadband dynamic stimuli, the correlation suggests that the psychophysical effect may be used as a reliable proxy of a general change of cortical excitability, which can be measured by fMRI.

### Monocular deprivation shifts BOLD Spatial Frequency Tuning for the deprived eye

For technical reasons, intrinsic to Binocular Rivarly, the monocular deprivation plasticity effect has previously measured only for foveal and high spatial frequencies stimuli – because these are the optimal conditions to measure binocular rivalry (44, 45). The BOLD measure gives us the chance to measure the effect of Monocular Deprivation across spatial frequencies and as function of eccentricity.

We used 5 different band-pass noise (1.25 octaves half-width at half maximum) stimuli with peak spatial frequency selected to have a complete coverage of spatial frequencies from 0.03 to 12.5 cpd (see Supplementary Fig. S2). Fig. 4 shows the BOLD responses elicited across the four conditions.

BOLD responses are medians across all V1 vertices (like in Fig. 1C), averaged across subjects. Before deprivation, the BOLD response shows a broad band-pass selectivity for our stimuli, with a preference for the stimulus peaking around 1 cpd, and a slight attenuation at higher spatial frequencies, similar for the two eyes (Fig. 4A&B). After deprivation, the non-deprived eye shows similar selectivity and an overall decrease of responses (Fig. 4C). For the deprived eye, there is no overall change of responsivity. However, the shape of the curve changes for the deprived eye: from band-pass to high-pass, implying that the enhancement affects primarily the higher spatial frequencies (Fig. 4D).

To model the effect at the individual vertex level, we assume that each vertex subtends a multitude of neuronal channels, each with narrow tuning for spatial frequency and collectively spanning a large range of spatial frequencies. Independently of the exact bandwidth and peak preference of the neuronal population contributing to the final BOLD selectivity, we find that the shape of all these curves is captured with a simple one-parameter model: what we term the population tuning for Spatial Frequency. This is given by a Difference-of-Gaussians (DoG) function with one free parameter, the spatial constant (while the excitation/inhibition spatial constant ratio is fixed; see eq. 4 in the Methods and curves in Supplementary Fig. S3). The free parameter sets the high spatial frequency cut-off at half-height of the filter. The continuous lines in Fig. 4 show how the model fits the grand-average of V1 responses, with best fit cut-off around 5 cpd similar for all conditions except for the POST-deprivation deprived eye, where the cut-off is 6.2 cpd (single vertex examples are given in supplementary Fig. S3C-I). The DoG equation has been successfully used in previous studies to model CSF and neural responses at variable stimulus parameters e.g. illumination levels (46, 47), validating this equation for modeling the overall selectivity of large neuronal ensembles.

Using this model to analyze single vertex responses, we evaluated the best-fit spatial frequency cut-off of the neural population contributing to the vertex BOLD response (see details in the methods and Supplementary Fig. S3A-C; briefly, we used the DoG model to predict the response elicited by our five band-pass noise stimuli in populations with different spatial frequency selectivity, i.e. filters with different cut-off; we then found the cut-off value that maximizes the correlation between the predicted responses and the observed BOLD responses). We used this procedure to fit BOLD responses in each of our four conditions, estimating spatial frequency selectivity in individual vertices in each condition: separately for the two eyes, PRE/POST deprivation. Before deprivation, the spatial frequency cut-off decays with eccentricity as expected. Fig 5A maps both eccentricity (pRF eccentricity estimates from a separate retinotopic mapping scan) and spatial frequency cut-off values, obtained by fitting responses to the deprived eye, before deprivation for (averaged across

hemispheres and subjects). The cut-off is around 16 in the para-fovea (eccentricity around 1.5 deg) and down to 4 in the periphery (eccentricity around 8 deg). This relationship between eccentricity and spatial frequency preference is consistent with previous fMRI results (48, 49) and with psychophysics (50). Fig. 5B shows how the model captures well (goodness of fit better than 0.9) the selectivity of an example V1 vertex, sampled from the mid-periphery (3.4 deg) for the deprived eye, both before and after deprivation. The spatial frequency cut-off after deprivation shifts to higher values, increasing (in this example) by about a factor of three. Fig. 5C-D shows that this behavior is systematically observed across V1 vertices. Here the average cut-off is plotted as function of eccentricity, and the roll-off is consistent with the map in Fig. 5A. For the deprived eye (Fig. 5D), at all eccentricities, there is a shift towards preferring higher spatial frequencies, which is captured by increased cut-off frequency, whereas there is no effect of deprivation for the non-deprived eye (Fig. 5C). To test the significance of these effects, we pooled the best fit cut-off values from all selected V1 vertices across eccentricities and averaged them across participants (Fig. 6A). The repeated measure ANOVA (performed on the log-transformed values, which are distributed normally as assessed by the Jarque-Bera test) shows no significant *time* × *eye* interaction ($F(1,17) = 3.13340$, $p = 0.09463$) and non significant main effect of time ($F(1,17) = 2.38678$, $p = 0.14078$) but a significant main effect of eye ($F(1,17) = 11.82278$, $p = 0.00314$). This is clarified by post-hoc t-tests revealing that the increase of spatial frequency cut-off for the deprived eye is significant ($t(17) = 2.118$, $p = 0.049$) whereas there is no significant change for the non-deprived eye ($t(17) = 0.370$, $p = 0.716$). Given that the *time* × *eye* interaction in the full V1 region is not significant, and to minimize noise contamination, we evaluated the effect of deprivation on spatial frequency cut-off at the individual level by a "Deprived Eye Change ($DepC_{cutoff}$)" index (Eq.7 in the methods), i.e. taking the POST vs. PRE-deprivation ratio of the spatial frequency cut-off for the deprived eye alone. As this ratio varies widely across participants, over more than 3 octaves, we asked whether this variability correlates with our psychophysical probe of plasticity: binocular rivalry. We used the same Eq. 7 to index the psychophysical change of the deprived eye ($DepC_{psycho}$), the POST to PRE- ratio of mean phase duration for the deprived eye, and found a strong positive correlation (Fig. 6B). POST-deprivation, the deprived eye shows an increase of mean phase duration (in binocular rivalry) and an increase of the spatial frequency cut-off (best fit of the BOLD responses): participants showing a stronger increase of phase duration, also showed a larger shift of selectivity towards higher spatial frequency. The correlation is consistent with the result of Fig. 3-4 showing that the enhancement of BOLD responses is correlated with the change of binocular rivalry and selective for the highest spatial frequency stimulus.

This suggests that MD plasticity induces a change of neural selectivity, not merely a change of overall responsivity, and probably a functional re-arrangement of the local cortical circuitry underlying ocular dominance.

## Discussion

We demonstrate that short-term abnormal visual experience profoundly impacts on V1 processing. BOLD activity across the V1 cortical region paradoxically increases for the eye that was deprived of vision, and decreases for the eye exposed to normal visual experience. This change of BOLD responsiveness is accompanied by a change of stimulus selectivity, specific for the deprived eye. The spatial frequency selectivity of individual V1 vertices becomes broader to encompass higher spatial frequencies. Prior psychophysical studies have shown that deprivation of form vision shifts eye dominance in favor of the deprived eye for small centrally presented targets, but the effect is short-lived, attenuated by more than 50% within the first 10 minutes (28, 29). It is a challenge to be able to detect such short-lived effect with BOLD. However, the high SNR of our ultra-high field MR scanner provided us with reliable signals with just two stimulus presentations.

The enhanced response in the deprived eye contrasts with the established result that brief deprivation during the critical period (2, 6-8) and long-term deprivation in adulthood (9) leads to the weakening of the deprived sense, e.g. the deprived eye. However, this fits well with the concept of homeostatic plasticity that was introduced only very recently in animal work during the developmental period (34, 35), and from our previous studies (26-29). Homeostatic plasticity acts upon the excitation-inhibition ratio, probably regulated by intra-cortical circuitry (33, 37), boosting of the response-gain for the circuitry with lower firing rates during deprivation. The present BOLD results validate this prediction in adult human and for short-term deprivation.

We believe that the modulation of BOLD responses we find is a probe of local cortical plasticity, not a mere consequence of visual adaptation. First, the deprivation was not complete, leaving luminance information – hence luminance adaptation – unaffected. Second, the BOLD response to the non-deprived eye is reduced, yet this eye receives normal visual input for the two hours, which cannot lead to contrast adaptation. Third, contrast adaptation or release thereof, is not consistent with the shift of preference towards higher spatial frequency that we observe for the deprived eye (see Fig. 6A). Finally, the boost of responses to the deprived eye and the suppression of the non-deprived eye are symmetric only for the highest spatial frequency stimulus, while at lower spatial frequencies the non-deprived eye alone is affected (suppressed; see Fig. 4A-C to appreciate the

suppression of the non-deprived eye at both low and high spatial frequencies); on the contrary, contrast adaptation mechanisms are expected to produce symmetrical effects across the spatial frequency range tested here. For all these reasons, adaptation cannot account for the present results.

Primary sensory cortex is generally resilient to plastic changes in adults, with more prominent effects in associative higher-level areas (51). The perceptual learning literature, which is the main paradigm for studying adult sensory plasticity, suggests that long term plasticity effects are more prominent in associative areas (13, 18), questioning the original idea that V1 circuitry can be optimized by perceptual experience (15). Our paradigm is very different from perceptual learning, having short-term consequences and being independent of perceptual decisions; our data clearly show that V1 circuitry can change with abnormal visual experience. Here, for the first time, we observe that the effect is localized in V1: affecting the entire V1 territory, with central and peripheral visual field representations equally affected. This help explaining previous behavioral evidence that MD affects the duration of suppression during binocular rivalry signal(29) – given that suppressed has been suggested to occur primary visual cortex (52). It also helps explaining the short-latency modulation of VEPs after MD(27), which cannot be directly associated with activity of any particular cortical area. Again for the first time, our results show that monocular deprivation effects are highly selective for eye and spatial frequency tuning: two properties that are most segregated in V1 neural populations. Later in higher level areas, circuits are usually binocular and have broader spatial frequency selectivity, implying that the MD effects should be more unspecific hence more difficult to reveal by testing ocular dominance. Despite the fact that BOLD responses always integrate feed-forward and feed-back input, making it difficult to localize the origin of modulations, the combination of all our results strongly suggest that the plasticity effect originate in V1.

Both BOLD amplitude modulation and the broadening of spatial frequency tuning for the deprived eye are observed across the V1 region, at all eccentricities. This leads to a surprising increase of BOLD acuity for the deprived eye at all eccentricities. Vertices with peak sensitivity at mid-to-low spatial frequencies shift to prefer the highest spatial frequency stimulus after deprivation. These are the majority of vertices in the visual periphery, where our estimates of acuity change is most reliable. Our procedure is likely to underestimate the change of acuity in the fovea, where many vertices already prefer the highest spatial frequency stimulus before deprivation. Notably, at all eccentricities, the acuity for the non-deprived eye is unaffected, corroborating the fact that the acuity change cannot result from a mere BOLD response amplitude changes (present for both eyes, in opposite direction) or the mere repetition of the sequence.

The antagonistic change of BOLD responses to the highest spatial frequency stimulus for the two eyes (suppressed for the non-deprived, boosted for the deprived) suggests a shift of ocular dominance in many V1 vertices. As shown by the histograms in Fig. 2, many of the voxels preferring the non-deprived eye before deprivation, shift to prefer the other eye after deprivation: a swap of ocular dominance. Strikingly, there is no such shift for vertices that already prefer the deprived eye before deprivation. If plasticity were not eye-specific and/or we failed to match our V1 vertices before/after deprivation, we would expect that splitting the distribution of V1 ocular dominance would generate opposite effects in the two subpopulations: vertices preferring the deprived eye before deprivation should swap to prefer the other eye, mirroring the effect seen in the vertices preferring non-deprived eye. This is not seen, implying first that we did successfully match vertices across the 2h of deprivation and more importantly that the selective Ocular Dominance shift, observed for about half of our vertices, is a genuine effect not an artifact.

A standard model of homeostatic plasticity is gain response modulation (33): one eye decreasing and the other increasing responsiveness. This models well the BOLD response in voxels preferring the non-deprived eye, but fails to capture the behavior of vertices preferring the deprived eye, which do not increase their preference but simply keep it the same as before deprivation. Thus, our Ocular Dominance data are not consistent with the idea of an overall gain increase for response to the deprived eye across all V1 vertices; rather, they are more consistent with the idea that representation for the deprived eye recruits after deprivation cortical resources normally dedicated to the other eye. In principle, this may well be associated with a recruitment of cortical territory, inducing a relative size change of ocular dominance columns. Here we did not attempt to map ocular dominance columns (53, 54), which is challenging even at ultra-high field and requires small voxel sizes and long acquisition times that would have been incompatible with the high SNR necessary to track our short-lived plasticity effect.

This hypothesis of functional recruitment of resources is also supported by the increased BOLD acuity for spatial frequency that we observed after deprivation. Our model assumes that each vertex samples from a population of neurons, each with different spatial frequency preference. After deprivation, the representation of the deprived eye enlarges by recruiting resources normally dedicated to the other eye; this expands the bandwidth which, for our stimulus set, implies an increase of BOLD acuity. In this light, a recruitment model is able to explain the antagonistic BOLD modulation for the deprived and non-deprived eye, the consequent shift of eye dominance, and increased acuity for the deprived eye. Although the recruitment model can account for many of our results, two of the observed effects are not easily captured. First, we do not see a symmetric

reduction of acuity for the non-deprived eye, which would have been expected from a reduction of the pool of spatial frequency channels. Second, we find that the BOLD response change is not always symmetric for the two eyes, with low spatial frequency responses being attenuated for the non-deprived eye and unchanged for the deprived eye (Figure 4). It is possible that plasticity is mediated by multiple coordinated mechanisms of different origin, which modulate not only gain and recruitment, but also selectivity bandwidth. Also, a decrease of neuronal selectivity for the deprived eye, often observed during plastic changes in animal models, can lead to both a shift of eye preference and an enlargement of spatial frequency tuning providing an alternative explanation of the major results reported here. Interestingly, a broadening of neuronal tuning is consistent with the reduced GABAergic inhibition (42), which is thought to accompany plasticity. This is supported by evidence in animal models (55, 56) and by MR Spectroscopy in humans where some of us demonstrated that short-term MD induces a change of resting GABA concentration (26). The GABA reduction correlated with the psychophysical estimates of ocular dominance shift, measured for central vision with binocular rivalry (26). However, the GABA modulation was observed in absence of visual stimulus and may be related to an unspecific neuromodulation of plasticity difficult to relate to neuronal processing.

Here, BOLD measurements allow us to evaluate the specific effects of MD on ocular dominance and spatial frequency channels. Both these effects correlate with our psychophysical plasticity assay based on binocular rivalry. Note that the correlation holds even though we pool BOLD responses and spatial frequency cut-off values across the entire V1 region of interest, whereas binocular rivalry is a specific measure of central vision. This implies that the change of binocular rivalry dynamics is a proxy for the more general plasticity effects that involves the whole primary visual cortex. Interestingly, the binocular rivalry phenomenon originates in the primary visual cortex – probably at the earliest stages – and is an expression of the dynamics of excitatory transmission and inhibitory feedback (57); as such it is a measure that could reflect the overall excitation-inhibition ratio (58). This recurrent excitatory/inhibitory circuitry could provide the common ground that relates rivalry in the central visual field and plasticity across V1. The implication of this finding has large potential as it could validate the use of binocular rivalry as a biomarker of adult cortical plasticity. Binocular Rivalry balance could become a simple non-invasive index of plasticity across clinical population and in adverse physiological conditions.

Understanding the residual plastic potential is important if we aim to re-open the critical period after insult. Particularly important is ocular dominance plasticity in amblyopia (59), a cortical deficit still without cure in adults, although recent advancements in training procedures are opening

new hopes (60, 61). Endorsing plasticity may increase the effectiveness of these treatments and preliminary data from our laboratory suggest that monocular deprivation of the amblyopic eye may indeed boost sensitivity of the deprived eye and improve its acuity (62) – exactly as observed in our BOLD results in normally sighted participants. Although sensory primary cortices are particularly resilient to plastic change in adult, our data demonstrate that 2h of abnormally unbalanced visual experience induce a functional reorganization of cortical circuits, leading to a change of ocular dominance and spatial frequency representation: the basic building blocks of V1 processing.

## Methods text

### EXPERIMENTAL MODEL AND SUBJECT DETAILS

#### *Human subjects*

Experimental procedures are in line with the declaration of Helsinki and were approved by the regional ethics committee [Comitato Etico Pediatrico Regionale—Azienda Ospedaliero-Universitaria Meyer—Firenze (FI)] and by the Italian Ministry of Health, under the protocol "Plasticità e multimodalità delle prime aree visive: studio in risonanza magnetica a campo ultra alto (7T)".

Twenty healthy volunteers with normal or corrected-to-normal visual acuity were examined (8 females and 12 males, mean age = 27 years) after giving written informed consent.

### METHOD DETAILS

#### *Experimental design*

Each participant underwent two scanning sessions separated by two hours, during which they were subject to the short-term monocular deprivation procedure described below. Just before each scanning section, their binocular rivalry was measured psychophysically. Data from one (male) participant was discarded from the analyses because of excessive head movements during the scan. Another (male) observer was excluded because of strong eye dominance tested with binocular rivalry before the deprivation. This left 18 participants (8 females and 10 males) whose complete datasets were entered all analyses. Sample size was set to enable testing for correlations between neuroimaging and psychophysical data. Previous work (26) reveals a correlation between MR spectroscopy data and binocular rivalry measures r = 0.62 (or higher), which implies a minimum of 17 participants to detect a significant correlation at 0.05 significance level, with test power of 80%(63).

### *Short-term Monocular Deprivation*

Monocular deprivation was achieved by patching the dominant eye for 2 hours. The operational definition of dominant eye applied to the eye showing the longer phase durations during the baseline binocular rivalry measurements. Like in previous studies (28-30), we used a translucent eye-patch made of plastic material allowing light to reach the retina (attenuation 15%), but preventing pattern vision, as assessed by the Fourier transform of a natural world image seen through the eye-patch. During the 2 hours of monocular deprivation, observers were free to read and use a computer.

### *Binocular Rivarly*

Binocular rivalry was measured in two short sessions (each comprising two runs of 3 minutes each), immediately before the Pre- and Post-deprivation MR sessions, in a quiet space adjacent to the MR control room. Visual stimuli were created in MATLAB running on a laptop (Dell) using PsychToolbox (64), and displayed on a 15- inch monitor (BenQ). Like in (26), observers viewed the visual stimuli presented on the monitor at a distance of 57 cm through anaglyph red-blue goggles (right lens blue, left lens red). Responses were recorded with the computer keyboard by continuous alternate keypresses. Visual stimuli were two oblique orthogonal red and blue gratings (orientation: ±45°, size: 3°, spatial frequency: 2 cpd, contrast 50%), surrounded by a white smoothed circle, presented on a black uniform background in central vision. Peak luminance of the red grating was reduced to match the peak luminance of the blue one using photometric measures. All included participants had typical binocular rivalry dynamics, with low percentage of mixed percepts (reported for 8.5 ± 2.04% of time on average). Only one participant experienced of mixed percepts for more than 20% of time (exactly for 31.2%) and his data are in line with the others'.

### *Stimuli for fMRI*

Visual stimuli were projected with an MR-compatible goggle set (VisuaStimDigital, Resonance Technologies, Los Angeles, USA), connected to a computer placed in the control room. The goggles covered a visual field of approximately 32 × 24 deg, with a resolution of 800 × 600 pixels, mean luminance 25 cd/m$^2$; the images in the two eyes were controlled independently.

During all functional MRI scans participants were instructed to maintain central fixation on a red point (0.5 degrees) that was constantly visible at the center of the screen. Bandpass noise stimuli were white noise images filtered to match the spatial frequency tuning of neurons in the visual cortex (65). We generated a large white noise matrix (8000 × 6000) and filtered it with a two-dimensional circular bandpass filter *Bp* defined by Eq. 1:

$$Bp = e^{\frac{-\ln\left(\frac{w}{P}\right)^2}{2[q*ln(2)]^2}} \quad \text{eq. 1}$$

where $P$ is the peak spatial frequency, $q$ is the filter half-width at half maximum in octaves. We generated five band-pass noise stimuli, by setting $q$ = 1.25 octaves and $P$ = 0.1 cpd, 0.2 cpd, 0.4 cpd, 1.1 cpd, 2.7 cpd. Each stimulus was presented for a block of 3TRs, during which the image was refreshed at 8Hz (randomly resampling a 800 × 600 window from the original matrix). Stimuli were scaled to exploit the luminance range of the display, and this yielded very similar RMS contrast values (shown in supplementary Fig. S2). Stimulus blocks were separated by 4TRs blanks, consisting of a mid-level gray screen. The five band-pass noise stimuli blocks were presented in pseudo-random order, twice per run, for a total of 70 TRs. In each run, stimuli were only presented to one eye, while the other was shown a mid-level gray screen. Each eye was tested once, before and after deprivation.

Immediately upon application of the monocular patch, we performed two additional scans to perform retinotopic mapping of visual areas. Meridian and ring stimuli were presented monocularly (to the non-patched eye) and were defined as apertures of a mid-level gray mask that uncovered a checkerboard pattern, 1 deg at 1 deg eccentricity to 2.5 deg at 9 deg eccentricity, rotating and contracting at a rate of one check per second. Meridians were defined by two 45° wedges centered around 0° or around 90°. The horizontal and vertical meridian were presented interchangeably for 5 TRs each (without blanks) and the sequence was repeated 6 times for a total of 60 TRs. Rings partitioned screen space into six contiguous eccentricity bands (0-0.9 deg, 0.9-1.8 deg, 1.8-3.3 deg, 3.3-4.7 deg, 4.7-6.48 deg, 6.48-9 deg). Odd and even rings were presented in two separate runs. In each run, the three selected rings and one blank were presented in random order for 5 TRs each, and the sequence was repeated (with different order) 6 times for a total of 120 TRs.

### *MR system and sequences*

Scanning was performed on a Discovery MR950 7 T whole body MRI system (GE Healthcare, Milwaukee, WI, USA) equipped with a 2-channel transmit driven in quadrature mode, a 32-channel receive coil (Nova Medical, Wilmington, MA, USA) and a high-performance gradient system (50 mT/m maximum amplitude and 200 mT/m/ms slew rate).

Anatomical images were acquired at 1 mm isotropic resolution using a T1-weighted magnetization-prepared fast Fast Spoiled Gradient Echo (FSPGR) with the following parameters: TR = 6 ms, TE = 2.2 ms. FA=12 deg, rBW = 50kHz, TI = 450 ms, ASSET = 2.

Functional images were acquired with spatial resolution 1.5 mm and slice thickness 1.4 mm with slice spacing = 0.1 mm, TR = 3000 ms, TE = 23ms, rBW = 250 kHz, ASSET = 2, phase encoding direction AP-PA. No resampling was performed during the reconstruction. For each EPI sequence, we acquired 2 additional volumes with the reversed phase encoding direction.

## QUANTIFICATION AND STATISTICAL ANALYSIS

### *ROI definition*

Areas V1 and V2 were manually outlined for all participants using retinotopic data projected on surface models of white matter. The V1/V2 boundary was traced from the vertical/horizontal meridian flip superior/inferior to the calcarine sulcus, and the V2/V3 border from the subsequent opposite flip. Anterior and posterior boundaries of V1 and V2 were based on activation from foveal (0°-0.9°) and most peripheral (6.48°-9°) ring stimuli. Vertices were only included in the analyses if we successfully estimated their preferred eccentricity (see below "Population Receptive Field estimation) and this was larger than 1, for no reliable mapping could be obtained for the central-most part of the visual field.

### *Pre-processing of imaging data*

Analyses were performed mainly with Freesurfer v6.0.0, with some contributions of the SPM12 and BrainVoyager 20.6 and FSL version 5.0.10 (66) packages.

Anatomical images were corrected for intensity bias using SPM12 (67) and processed by a standard procedure for segmentation implemented in Freesurfer (recon-all: 68). In addition, each hemisphere was aligned to a left/right symmetric template hemisphere (fsaverage_sym: 69).

Functional images were corrected for subject movements (70) and undistorted using EPI images with reversed phase encoding direction (Brain Voyager COPE plug-in 71). We then exported the preprocessed images from BrainVoyager to NiFTi format. These were aligned to each participant's anatomical image using a boundary based registration algorithm (Freesurfer *bbergister* function) and projected to the cortical surface of each hemisphere. All analyses were conducted on data in the individual subject space. In addition, for visualization purposes, we also aligned the results of timecourse analyses (GLM and subsequent pRF and spatial frequency tuning estimates) to the left/right symmetric template hemisphere. Averaged results across the 18x2 hemispheres are shown in the maps of Fig. 1B, Fig. 5A and Supplementary Fig. S1.

### *GLM analysis of fMRI data*

General Linear Model analysis was performed with in-house MATLAB software (Mathworks, version R2016b). We assumed that fMRI timecourses result from the linear combination of N predictors: boxcar functions representing stimulus presence/absence (one per stimulus type) convolved by a standard hemodynamic response function (see Eq. 2), plus two nuisance variables (a linear trend and a constant). We modeled the hemodynamic response function as a gamma function h(t):

$$h(t) = \frac{\left(\frac{t-\delta}{\tau}\right)^{(n-1)} e^{-\left(\frac{t-\delta}{\tau}\right)}}{\tau(n-1)!} \qquad \text{eq. 2}$$

with parameters $n$=3, $t$=1.5 s, and d=2.25 s (72). Beta weights of the stimuli predictors were taken as estimates of the BOLD response amplitude and normalized by the predictor amplitude to obtain a measure that directly corresponds to % signal change; beta weights were also scaled by an error measure to obtain t-values, following the same procedure as in (73).

### *Population Receptive Field mapping*

The pRFs of the selected voxels were estimated with custom software in Matlab, implementing a method related to that described by Dumoulin and Wandell (74). We modeled the pRF with a 1D Gaussian function defined over eccentricity, with parameters $\varepsilon$ and $\sigma$ as mean and standard deviation respectively, and representing the aggregate receptive field of all neurons imaged within the vertex area. We defined the stimulus as a binary matrix S representing the presence of visual stimulation over space (here, eccentricity between 0 and 10 deg with 40 steps per deg) for each of 6 ring stimuli. We used the results of our GLM analysis to estimate the vertex response to each of our 6 rings (as t-values; using beta values yields very similar results). We assumed that each vertex response is the linear sum over space (eccentricity) of the overlap between the pRF of the voxel and the input stimulus, which is mathematically equivalent to the matrix multiplication between the stimulus and the pRF.

$$R_i = G(\varepsilon, \sigma) * S_i \qquad \text{eq. 3}$$

where $i$ is the index to ring number and varies between 1 and 6.

We used this equation to predict the response to our six rings for a large set of initial pRF parameters; for each vertex, we measured the correlation (our goodness-of-fit index) between the predicted response and the observed t-values. If the highest correlation was < .7 the vertex was

discarded; otherwise, the parameters yielding the highest correlation were used to initialize a nonlinear search procedure (MATLAB simplex algorithm), which manipulated $\varepsilon$ and $\sigma$ to maximize goodness-of-fit, with the constraint that $\varepsilon$ could not exceed 20 deg or be smaller than 1 deg, and $\sigma$ could not be smaller than .1 deg. Successful fits were obtained for 72.20 ± 1.95% of V1 vertices, for which the initial coarse grid search gave a correlation > 0.7 and the nonlinear search settled within the constraints. All analyses (on average and distribution of responses and tuning parameters) considered the sub-region of V1 for which a successful fit was obtained. We used $\varepsilon$ to estimate the preferred eccentricity of each vertex.

The main modifications of our procedure relative to that described by Dumoulin and Wandell (74) are the following: (a) fMRI data were acquired in a block design with only six stimulus types (six eccentricity bands) rather than varying stimulus position at each TR; this allowed us to use a standard GLM approach to estimate each vertex response to the six stimuli (assuming a standard hemodynamic response function) and then use the pRF model to predict these six time-points – much faster than predicting the full fMRI series of 120x2 TRs; (b) our stimuli and consequently our pRFs were defined in one dimension (eccentricity) – whereas the standard pRF is defined in 2D, eccentricity and polar angle (or Cartesian x and y); (c) we maximized the correlation between the predicted and observed fMRI response time-courses rather than minimizing the root mean square error; this eliminates the need to estimate a scale factor to account for the unknown units of the BOLD signal.

### *Population Tuning for Spatial Frequency*

Using a similar logic, we also estimated the population tuning for Spatial Frequency, which represents the aggregate Spatial Frequency tuning of the population of neurons imaged within each vertex area. We modeled the population tuning using a family of functions that includes the psychophysical Contrast Sensitivity Function (CSF) and can be specified by the following one-parameter equation (Difference-of-Gaussians):

$$pSFT = e^{\frac{-v^2}{\sigma}} - e^{\frac{-v^2}{\sigma/50}} \times \sigma \qquad \text{eq. 4}$$

Like we did for the pRF mapping, we defined a stimulus matrix S representing the Fourier spectra of our five bandpass noise stimuli, i.e. the energy of visual stimulation in the frequency domain (here, between 0.03 cpd and 12.5 cpd) for each stimulus. We used the results of our GLM analysis to estimate the vertex response to each of our five bandpass noise stimuli (as t-values; using beta values yields very similar results). We assumed that each vertex response is the linear sum over

frequency of the overlap between the pSFT of the voxel and the input stimulus, which is mathematically equivalent to the matrix multiplication between the stimulus and the pSFT.

Like for pRFs, we estimated the best-fit $\sigma$ parameter of each vertex pSFT with a two-step procedure: a coarse-grid search followed by the simplex search. We used the matrix multiplication of the pSFT and the stimulus to predict the response to our five bandpass noise stimuli for a large set of initial $\sigma$ values (between 1 and 1,000 in 100 logarithmic steps); for each vertex, we measured the correlation (our goodness-of-fit index) between the predicted response and the observed t-values. If the highest correlation was < .5, the voxel was discarded, otherwise the parameter yielding the highest correlation were used to initialize a nonlinear search procedure (MATLAB simplex algorithm), which manipulated $\sigma$ to maximize goodness-of-fit, with the constraint that $\sigma$ could not be smaller than .3 and larger than 10,000. Successful fits were obtained for 89.53 ± 1.14% of V1 vertices for which we obtained a successful eccentricity fit (87.44 ± 1.12% of all V1 vertices).

We express the $\sigma$ parameter in terms of the high-spatial frequency cutoff of the filter (highest spatial frequency at half maximum), $SFco$ for each vertex:

$$^{SF}co = 1.26\sqrt{\frac{\sigma}{2}} - 0.045 \qquad \text{eq. 5}$$

### *Indices defining the effect of deprivation*

We computed the effects of short-term monocular deprivation on both the dynamics of binocular rivalry and our fMRI results, estimating the degree to which the two measures are correlated. In all cases, the same equation was applied to psychophysical and fMRI data.

The first index, called "Deprivation Index" or $DI_{psycho}$ and $DI_{BOLD}$ is given by eq. 6

$$DI = \left(\frac{y_{DepPOST}}{y_{DepPRE}}\right) \Big/ \left(\frac{y_{NdepPOST}}{y_{NdepPRE}}\right) \qquad \text{eq. 6}$$

For psychophysics, y = mean duration of Binocular Rivalry phases of the Dep or Ndep eye, during the PRE- or POST deprivation sessions; for fMRI, y = median BOLD response across V1 vertices to stimuli in the Dep or Ndep eye, during the PRE- or POST-deprivation sessions.

The second index, called "Deprived-eye change" or $DepC_{psycho}$ and $DepC_{cutoff}$ is given by eq. 7

$$DepC = \left(\frac{y_{DepPOST}}{y_{DepPRE}}\right) \quad \text{eq. 7}$$

For psychophysics, y = mean duration of Binocular Rivalry phases of the Dep eye, during the PRE- or POST deprivation sessions. For fMRI, y = mean spatial frequency cut-off across V1 vertices estimated for stimuli in the Dep eye, during the PRE- or POST-deprivation sessions.

### *Statistics*

Data from individual participants (mean binocular rivalry phase durations or median BOLD responses/pRF/pST across V1 or V2 vertices) were analyzed with a repeated measure ANOVA approach, after checking that distributions do not systematically deviate from normality by means of the Jarque-Bera test for composite normality (Matlab *jbtest* function, p-values given in the relevant figures). F statistics are reported with associated degrees of freedom and p-values in the Results section, in the form: $F(df,df_{err})$ = value; p = value. Post-hoc paired t-tests comparing conditions follow the ANOVA results, in the form: t(df) = value, p = value. Associations between variables are assessed with Pearson product-moment correlation coefficient, reported in the form: r(n) = value, p = value. Aggregate subject data (i.e. vertices pooled across participants and hemispheres) were typically non-normally distributed and thereby were analysed with non-parametric tests. The Wilcoxon sign-rank test was used for comparing medians, and results are reported in the form: z = value, p = value.

## DATA AND SOFTWARE AVAILABILITY

Data and software will be made available before the final submission.

## References


1. Pascual-Leone A, Amedi A, Fregni F, & Merabet LB (2005) The plastic human brain cortex. *Annu Rev Neurosci* 28:377-401.
2. Wiesel TN & Hubel DH (1963) Effects of Visual Deprivation on Morphology and Physiology of Cells in the Cats Lateral Geniculate Body. *J Neurophysiol* 26:978-993.
3. Hubel DH & Wiesel TN (1970) The period of susceptibility to the physiological effects of unilateral eye closure in kittens. *J Physiol* 206(2):419-436.
4. Hubel DH, Wiesel TN, & LeVay S (1977) Plasticity of ocular dominance columns in monkey striate cortex. *Philos Trans R Soc Lond B Biol Sci* 278(961):377-409.
5. Berardi N, Pizzorusso T, & Maffei L (2000) Critical periods during sensory development. *Curr Opin Neurobiol* 10(1):138-145.
6. Gordon JA & Stryker MP (1996) Experience-dependent plasticity of binocular responses in the primary visual cortex of the mouse. *J Neurosci* 16(10):3274-3286.

7. Kiorpes L, Kiper DC, O'Keefe LP, Cavanaugh JR, & Movshon JA (1998) Neuronal correlates of amblyopia in the visual cortex of macaque monkeys with experimental strabismus and anisometropia. *J Neurosci* 18(16):6411-6424.
8. Levi DM & Carkeet A (1993) Amblyopia: a consequence of abnormal visual development. *Early Visual Development, Normal and Abnormal*, ed Simons K (Oxford University Press, New York, NY), pp 391-408.
9. Sato M & Stryker MP (2008) Distinctive features of adult ocular dominance plasticity. *J Neurosci* 28(41):10278-10286.
10. Baseler HA*, et al.* (2011) Large-scale remapping of visual cortex is absent in adult humans with macular degeneration. *Nat Neurosci* 14(5):649-655.
11. Baseler HA*, et al.* (2002) Reorganization of human cortical maps caused by inherited photoreceptor abnormalities. *Nat Neurosci* 5(4):364-370.
12. Wandell BA & Smirnakis SM (2009) Plasticity and stability of visual field maps in adult primary visual cortex. *Nat Rev Neurosci* 10(12):873-884.
13. Dosher B & Lu ZL (2017) Visual Perceptual Learning and Models. *Annu Rev Vis Sci* 3:343-363.
14. Fahle M & Poggio T (2002) *Perceptual learning* (MIT Press, Cambridge).
15. Fiorentini A & Berardi N (1980) Perceptual learning specific for orientation and spatial frequency. *Nature* 287:43-44.
16. Karni A & Sagi D (1991) Where practice makes perfect in texture discrimination: evidence for primary visual cortex plasticity. *Proc Natl Acad Sci USA* 88(11):4966-4970.
17. Karni A & Sagi D (1993) The time course of learning a visual skill. *Nature* 365(6443):250-252.
18. Watanabe T & Sasaki Y (2015) Perceptual learning: toward a comprehensive theory. *Annu Rev Psychol* 66:197-221.
19. Dosher BA & Lu Z-L (1999) Mechanisms of perceptual learning. *Vision Res* 39(19):3197-3221.
20. Harris H, Gliksberg M, & Sagi D (2012) Generalized perceptual learning in the absence of sensory adaptation. *Curr Biol* 22(19):1813-1817.
21. Kahnt T, Grueschow M, Speck O, & Haynes JD (2011) Perceptual learning and decision-making in human medial frontal cortex. *Neuron* 70(3):549-559.
22. Karni A*, et al.* (1995) Functional MRI evidence for adult motor cortex plasticity during motor skill learning. *Nature* 377(6545):155-158.
23. Lewis CM, Baldassarre A, Committeri G, Romani GL, & Corbetta M (2009) Learning sculpts the spontaneous activity of the resting human brain. *Proc Natl Acad Sci U S A* 106(41):17558-17563.
24. Shibata K*, et al.* (2012) Decoding reveals plasticity in V3A as a result of motion perceptual learning. *PLoS One* 7(8):e44003.
25. Zhang P, Bao M, Kwon M, He S, & Engel SA (2009) Effects of orientation-specific visual deprivation induced with altered reality. *Curr Biol* 19(22):1956-1960.
26. Lunghi C, Emir UE, Morrone MC, & Bridge H (2015) Short-Term Monocular Deprivation Alters GABA in the Adult Human Visual Cortex. *Curr Biol* 25(11):1496-1501.
27. Lunghi C, Berchicci M, Morrone MC, & Di Russo F (2015) Short-term monocular deprivation alters early components of visual evoked potentials. *J Physiol* 593(19):4361-4372.
28. Lunghi C, Burr DC, & Morrone MC (2013) Long-term effects of monocular deprivation revealed with binocular rivalry gratings modulated in luminance and in color. *J Vis* 13(6).
29. Lunghi C, Burr DC, & Morrone C (2011) Brief periods of monocular deprivation disrupt ocular balance in human adult visual cortex. *Curr Biol* 21(14):R538-539.

30. Binda P & Lunghi C (2017) Short-Term Monocular Deprivation Enhances Physiological Pupillary Oscillations. *Neural Plast* 2017:6724631.
31. Zhou J, Reynaud A, & Hess RF (2014) Real-time modulation of perceptual eye dominance in humans. *Proc Biol Sci* 281(1795).
32. Zhou J, Clavagnier S, & Hess RF (2013) Short-term monocular deprivation strengthens the patched eye's contribution to binocular combination. *J Vis* 13(5).
33. Turrigiano G (2012) Homeostatic synaptic plasticity: local and global mechanisms for stabilizing neuronal function. *Cold Spring Harb Perspect Biol* 4(1):a005736.
34. Mrsic-Flogel TD*, et al.* (2007) Homeostatic regulation of eye-specific responses in visual cortex during ocular dominance plasticity. *Neuron* 54(6):961-972.
35. Turrigiano GG & Nelson SB (2004) Homeostatic plasticity in the developing nervous system. *Nat Rev Neurosci* 5(2):97-107.
36. Ranson A, Cheetham CE, Fox K, & Sengpiel F (2012) Homeostatic plasticity mechanisms are required for juvenile, but not adult, ocular dominance plasticity. *Proc Natl Acad Sci U S A* 109(4):1311-1316.
37. Maffei A & Turrigiano GG (2008) Multiple modes of network homeostasis in visual cortical layer 2/3. *J Neurosci* 28(17):4377-4384.
38. Merabet LB*, et al.* (2008) Rapid and reversible recruitment of early visual cortex for touch. *PLoS One* 3(8):e3046.
39. Pitskel NB, Merabet LB, Ramos-Estebanez C, Kauffman T, & Pascual-Leone A (2007) Time-dependent changes in cortical excitability after prolonged visual deprivation. *Neuroreport* 18(16):1703-1707.
40. Boroojerdi B, Battaglia F, Muellbacher W, & Cohen LG (2001) Mechanisms underlying rapid experience-dependent plasticity in the human visual cortex. *Proc Natl Acad Sci U S A* 98(25):14698-14701.
41. Boroojerdi B*, et al.* (2000) Enhanced excitability of the human visual cortex induced by short-term light deprivation. *Cereb Cortex* 10(5):529-534.
42. Priebe NJ & Ferster D (2008) Inhibition, spike threshold, and stimulus selectivity in primary visual cortex. *Neuron* 57(4):482-497.
43. Lunghi C & Sale A (2015) A cycling lane for brain rewiring. *Curr Biol* 25(23):R1122-1123.
44. Blake R, O'Shea RP, & Mueller TJ (1992) Spatial zones of binocular rivalry in central and peripheral vision. *Vis Neurosci* 8(5):469-478.
45. Kang MS & Blake R (2011) An integrated framework of spatiotemporal dynamics of binocular rivalry. *Front Hum Neurosci* 5:88.
46. Hawken MJ, Parker AJ, & Lund JS (1988) Laminar organization and contrast sensitivity of direction-selective cells in the striate cortex of the Old World monkey. *J Neurosci* 8(10):3541-3548.
47. Enroth-Cugell C & Robson JG (1966) The contrast sensitivity of retinal ganglion cells of the cat. *J Physiol* 187(3):517-552.
48. D'Souza DV, Auer T, Frahm J, Strasburger H, & Lee BB (2016) Dependence of chromatic responses in V1 on visual field eccentricity and spatial frequency: an fMRI study. *J Opt Soc Am A Opt Image Sci Vis* 33(3):A53-64.
49. Henriksson L, Nurminen L, Hyvarinen A, & Vanni S (2008) Spatial frequency tuning in human retinotopic visual areas. *J Vis* 8(10):5 1-13.
50. Rovamo J, Virsu V, & Nasanen R (1978) Cortical magnification factor predicts the photopic contrast sensitivity of peripheral vision. *Nature* 271(5640):54-56.
51. Fuchs E & Flugge G (2014) Adult neuroplasticity: more than 40 years of research. *Neural Plast* 2014:541870.

52. Sterzer P, Stein T, Ludwig K, Rothkirch M, & Hesselmann G (2014) Neural processing of visual information under interocular suppression: a critical review. *Front Psychol* 5:453.
53. Yacoub E, Shmuel A, Logothetis N, & Ugurbil K (2007) Robust detection of ocular dominance columns in humans using Hahn Spin Echo BOLD functional MRI at 7 Tesla. *Neuroimage* 37(4):1161-1177.
54. Cheng K, Waggoner RA, & Tanaka K (2001) Human ocular dominance columns as revealed by high-field functional magnetic resonance imaging. *Neuron* 32(2):359-374.
55. Heimel JA, van Versendaal D, & Levelt CN (2012) The role of GABAergic inhibition in ocular dominance plasticity. *Neural Plast* 2011:391763.
56. Baroncelli L, Maffei L, & Sale A (2011) New perspectives in amblyopia therapy on adults: a critical role for the excitatory/inhibitory balance. *Front Cell Neurosci* 5:25.
57. Tong F, Meng M, & Blake R (2006) Neural bases of binocular rivalry. *Trends Cogn Sci* 10(11):502-511.
58. van Loon AM*, et al.* (2013) GABA shapes the dynamics of bistable perception. *Curr Biol* 23(9):823-827.
59. Webber AL & Wood J (2005) Amblyopia: prevalence, natural history, functional effects and treatment. *Clin Exp Optom* 88(6):365-375.
60. Sengpiel F (2014) Plasticity of the visual cortex and treatment of amblyopia. *Curr Biol* 24(18):R936-940.
61. Levi DM & Li RW (2009) Improving the performance of the amblyopic visual system. *Philos Trans R Soc Lond B Biol Sci* 364(1515):399-407.
62. Lunghi C*, et al.* (2016) Short-term deprivation of the amblyopic eye, combined with physical exercise, promotes long-term visual recovery in adult anisometropic patients. *Neuroscience Meeting Planner. San Diego, CA: Society for Neuroscience. Online*.
63. Lachin JM (1981) Introduction to sample size determination and power analysis for clinical trials. *Control Clin Trials* 2(2):93-113.
64. Brainard DH (1997) The Psychophysics Toolbox. *Spat Vis* 10(4):433-436.
65. Morrone MC & Burr DC (1988) Feature detection in human vision: a phase-dependent energy model. *Proc R Soc Lond B Biol Sci* 235(1280):221-245.
66. Jenkinson M, Beckmann CF, Behrens TE, Woolrich MW, & Smith SM (2012) Fsl. *Neuroimage* 62(2):782-790.
67. Friston KJ (2007) *Statistical parametric mapping : the analysis of funtional brain images* (Elsevier/Academic Press, Amsterdam ; Boston) 1st Ed pp vii, 647 p.
68. Fischl B*, et al.* (2002) Whole brain segmentation: automated labeling of neuroanatomical structures in the human brain. *Neuron* 33(3):341-355.
69. Greve DN*, et al.* (2013) A surface-based analysis of language lateralization and cortical asymmetry. *J Cogn Neurosci* 25(9):1477-1492.
70. Goebel R, Esposito F, & Formisano E (2006) Analysis of functional image analysis contest (FIAC) data with brainvoyager QX: From single-subject to cortically aligned group general linear model analysis and self-organizing group independent component analysis. *Hum Brain Mapp* 27(5):392-401.
71. Jezzard P & Balaban RS (1995) Correction for geometric distortion in echo planar images from B0 field variations. *Magn Reson Med* 34(1):65-73.
72. Boynton GM, Engel SA, Glover GH, & Heeger DJ (1996) Linear systems analysis of functional magnetic resonance imaging in human V1. *J Neurosci* 16(13):4207-4221.
73. Friston KJ*, et al.* (1994) Statistical parametric maps in functional imaging: A general linear approach. *Human Brain Mapping* 2(4):189-210.

74. Dumoulin SO & Wandell BA (2008) Population receptive field estimates in human visual cortex. *Neuroimage* 39(2):647-660.

## Acknowledgments

This research was supported by the European Research Council under the European Union's Seventh Framework Programme (FPT/2007-2013) under grant agreement number 338866 (P.B., C.L., and M.C.M.) and under ERA-NET project "Neuro-DREAM" (C.L., and M.C.M.) and by the European Union's Horizon 2020 Research and Innovation Programme under the Marie Sklodowska-Curie grant agreement number 641805 (J.W.K.) and by the Italian Ministry of University and Resarch under the project PRIN2015 (M.C.M) and by Fondazione Roma under the Grants for Biomedical Research: Retinitis Pigmentosa (RP)-Call for proposals 2013- "Cortical Plasticity in Retinitis Pigmentosa: an Integrated Study from Animal Models to Humans". The authors would like to thank Mauro Costagli for help with the data acquisition.

## Author contributions

P.B., C.L., and M.C.M. designed the experiments. J.W.K., P.B., C.L. and L.B. performed the experiments and M.T. supervised the 7T scanning. P.B. and J.W.K. analyzed the results. P.B. and M.C.M. wrote the manuscript. All authors revised the manuscript.

## Competing of Interests

The authors declare no competing interests.

## Materials and correspondence

Correspondence should be addressed to Maria Concetta Morrone concetta@in.cnr.it

## Figure legends

### Figure 1: Monocular deprivation modulates 7T BOLD responses in early visual cortex

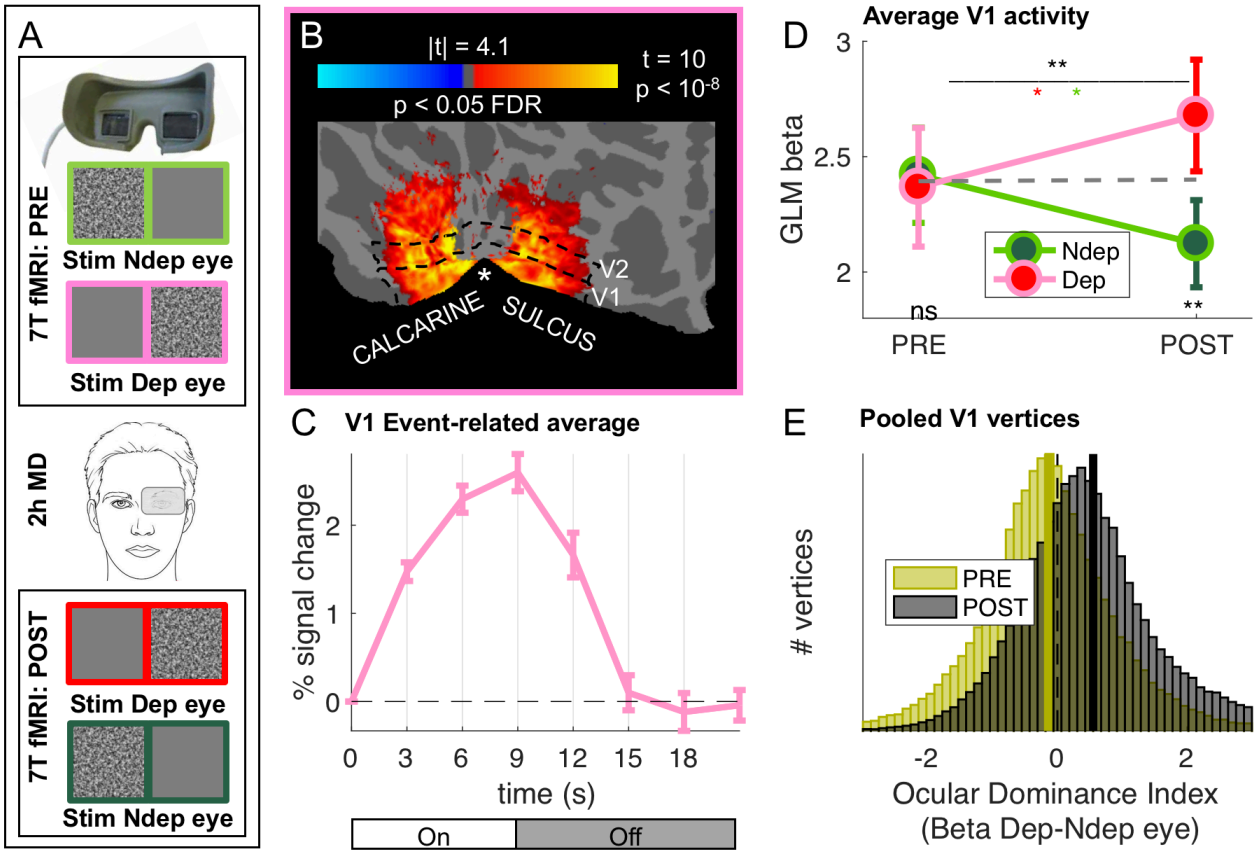


A: Schematic illustration of the methods. The icons show a band-pass noise stimulus shown to either eye through the MR compatible goggles. Before and after the Pre- and Post-deprivation scans, outside the bore, we also measured binocular rivalry.

B: BOLD responses evoked by our band-pass noise stimulus with peak frequency 2.7 cycles per degree (cpd), presented in the deprived eye PRE-deprivation, mapped on the flattened cortical surface, cut at the calcarine sulcus. T-values are obtained by aligning GLM betas for each subject and hemisphere to a left/right symmetric template hemisphere, excluding vertices for which preferred eccentricity was not adequately estimated or smaller than 1 (the same criterion used for al analyses), then evaluating the distribution of betas in each vertex against 0 (one-sample t-test) and FDR correcting across the entire cortical surface. Black dashed lines mark the borders of the V1 and V2 regions representing the screen space (24 x 32deg), with * marking the fovea.

C: BOLD modulation during the 3 TRs of stimulus presentation (from 0 to 9s) and the following 4 blank TRs, for the 2.7 cpd noise stimuli delivered to the deprived eye before deprivation. The y-axis show the median percent BOLD signal change in V1 vertices relative to the signal at stimulus onset, averaged across subjects. Error bars give s.e. across participants.

D: Average BOLD response to the band-pass noise stimulus with peak frequency 2.7 cpd, in each of the four conditions, computed by taking the median BOLD response across all V1 vertices then averaging these values across participants (after checking that distributions do not deviate from normality, Jarque-Bera hypothesis test of composite normality, all $p > 0.06$). The top black star indicates the significance of the ANOVA interaction between factors *time* (PRE, POST deprivation) and *eye* (deprived, non-deprived); the other stars report the results of post-hoc t-tests: red and green stars give the significance of the difference POST minus PRE, for the deprived and non-deprived eye respectively; bottom black stars give the significance of the difference deprived minus non-deprived eye before and after deprivation. * $p<0.05$; ** $p < 0.01$; *** $p < 0.001$; *ns* non-significant.

E: Histograms of Ocular Dominance Index: the difference between the response (GLM beta) to the deprived and non-deprived eye, computed for each vertex, separately before and after deprivation. Yellow and black lines give the median of the distributions, which are non-normal (logistic) due to excess kurtosis.

Figure 2: Monocular deprivation shifts 7T BOLD Ocular Dominance in V1

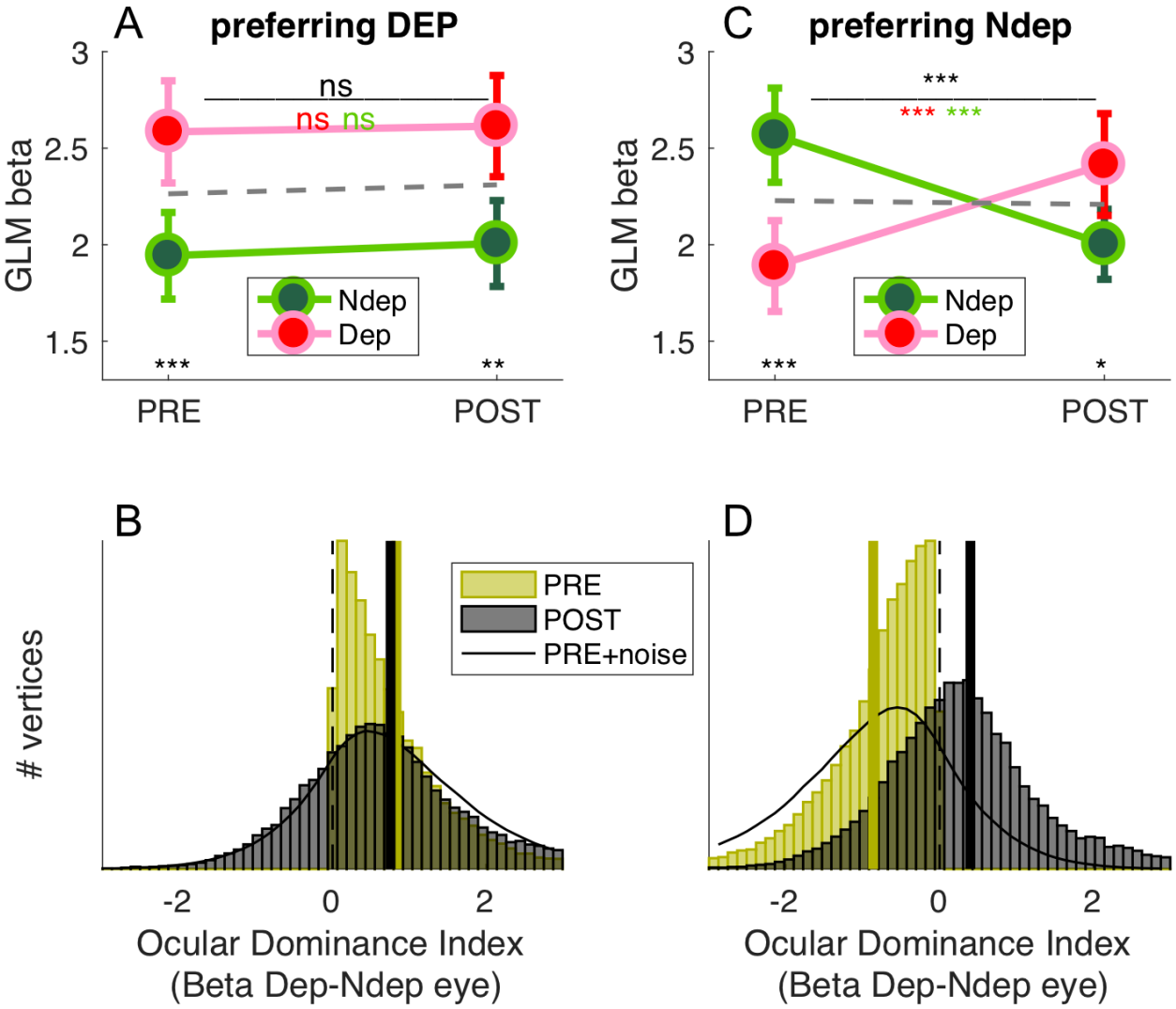


A & C: Average BOLD responses with the same conventions as in Fig. 1D but analysing data from two sub-regions of V1. A: only vertices that, before deprivation, respond preferentially to the deprived eye. C: only vertices that, before deprivation, respond preferentially to the non-deprived eye.

B & D: Histograms of Ocular Dominance Index (as for Fig. 1E), in the two sub-regions of V1, computed before and after deprivation. The black curve simulates the result of adding random noise to the distribution obtained before deprivation; only in B does this approximate the distribution observed after deprivation.

Figure 3: Deprivation effects on BOLD and on psychophysics are correlated

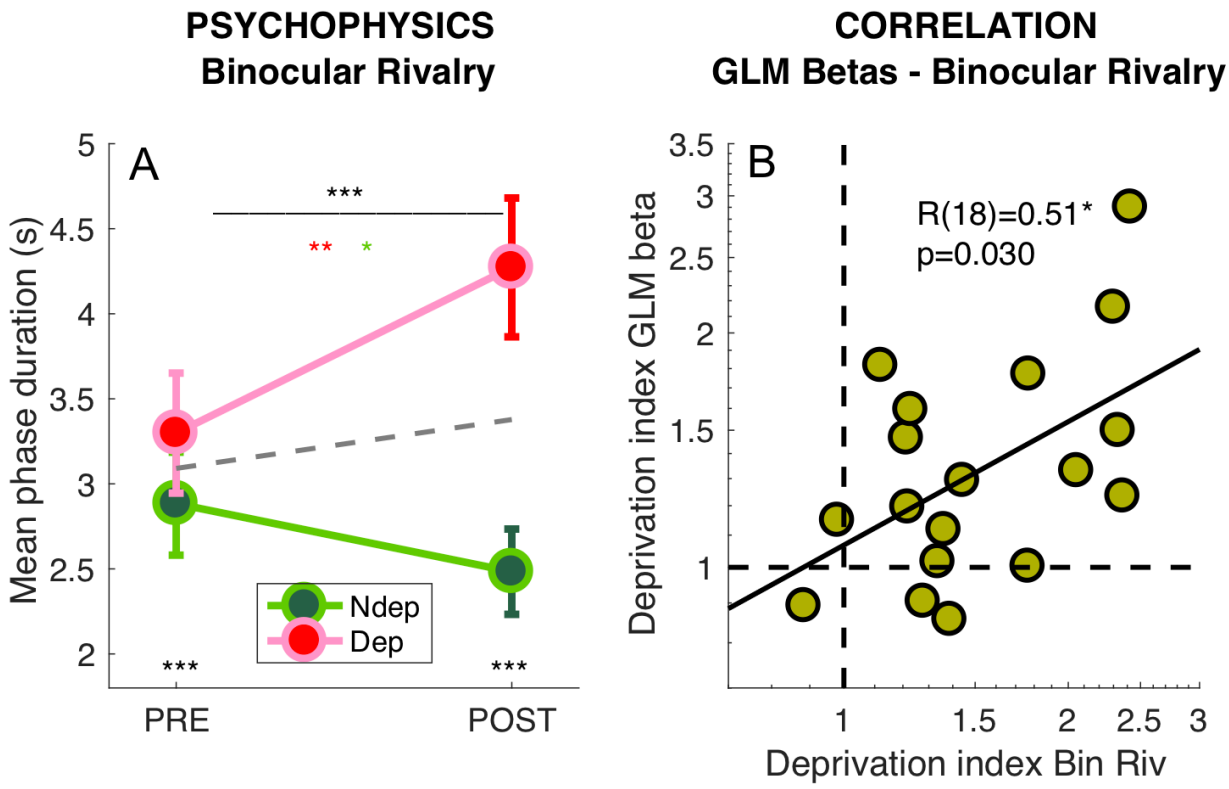


A: Effect of deprivation on Binocular Rivalry dynamics. Average phase duration for the deprived and non-deprived eye, before and after deprivation, same conventions as in Fig.1D. Mean phase duration distributions do not deviate from normality (Jarque-Bera hypothesis test of composite normality, all $p > 0.171$)

B: Correlation between the deprivation index (the POST to PRE- ratio for the deprived eye divided by the same ratio for the non-deprived eye, Eq. 6 in Methods) computed for the binocular rivalry mean phase duration and for the BOLD response to our band-pass noise stimulus with peak frequency 2.7 cpd. Text insets show the Pearson's correlation coefficient and associated p-value.

Figure 4: Deprivation affects spatial frequency selectivity in V1

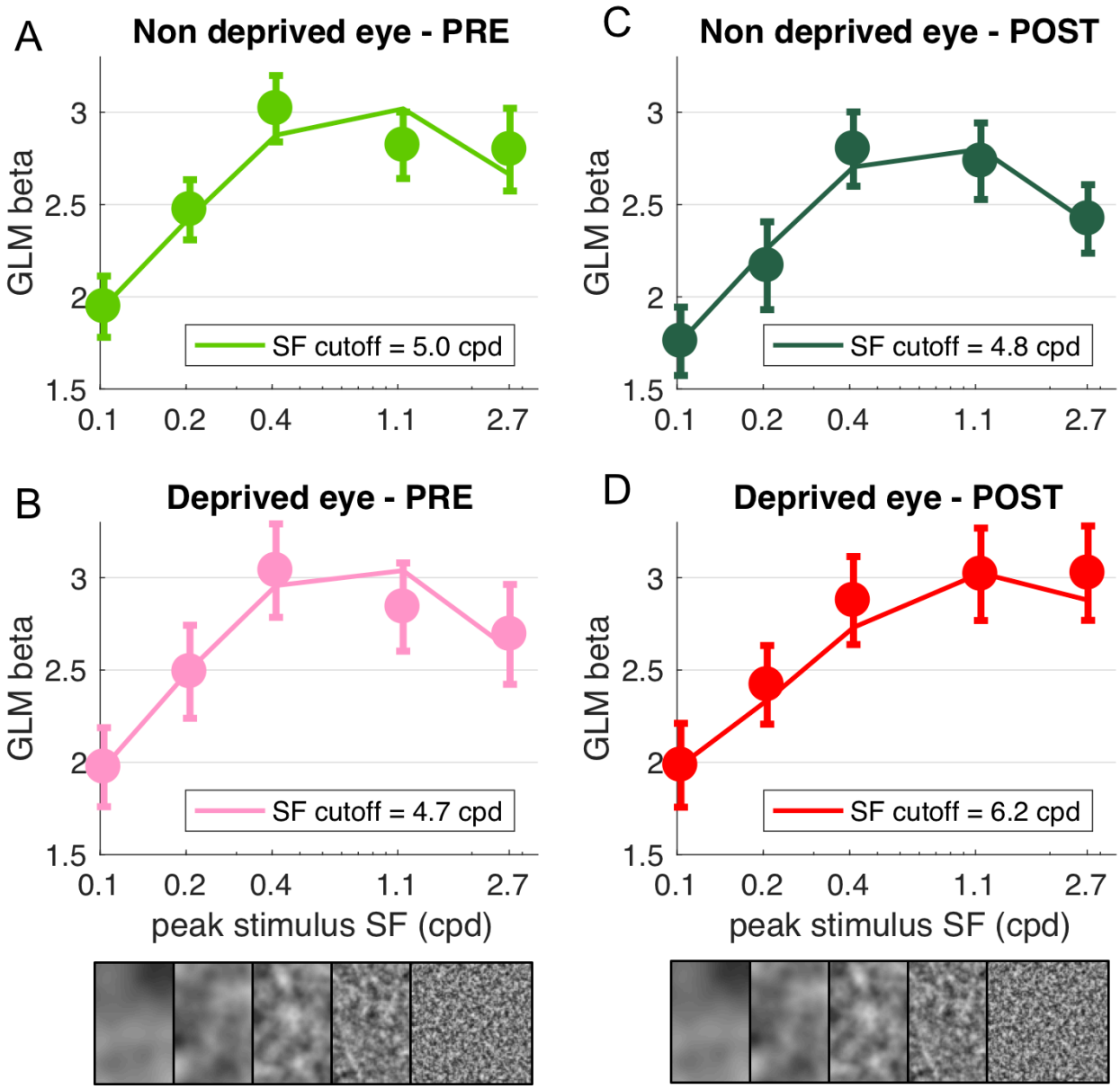


Average V1 BOLD responses to all five of our band-pass noise stimuli (with peaks at 0.1, 0.2, 0.4, 1.1 and 2.7 cpd, see spectra in supplementary Fig. S2). Continuous lines show the response of the best-fit population Spatial Frequency tuning (with the one parameter, the high spatial frequency cut-off, indicated in the legend), estimated by applying to the average V1 BOLD response the same model used to predict individual vertex responses (fitting procedure illustrated in supplementary Fig. S3).

Figure 5: population Spatial Frequency Tuning in V1

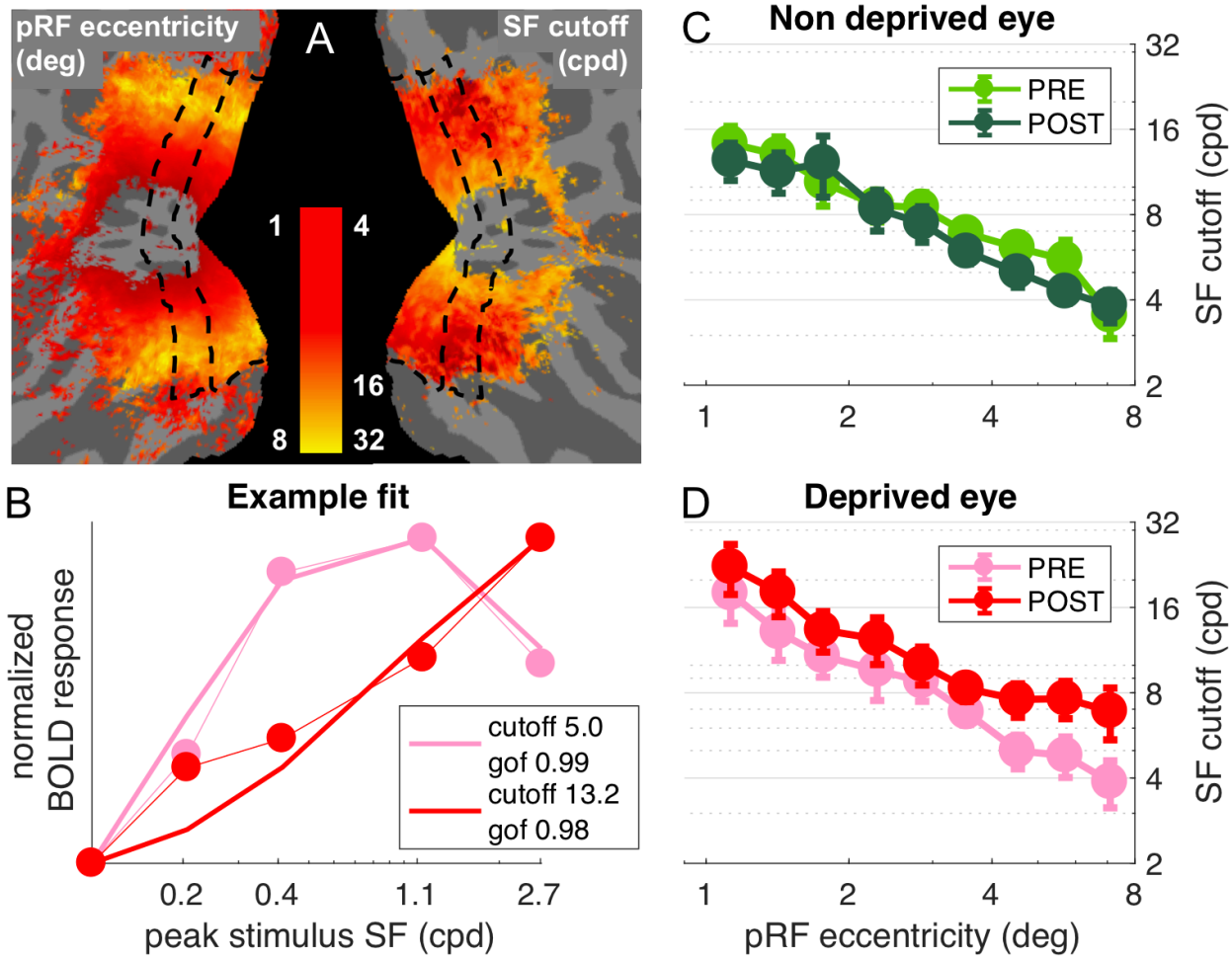


A: Maps of pRF eccentricity and best fit spatial frequency cut off (for the deprived eye before deprivation) after aligning the parameter estimates for all hemispheres to a common template and averaging them across subjects and hemispheres, after excluding vertices for which the average preferred eccentricity was not adequately estimated or smaller than 1 (the same exclusion criteria used for analyses).

B: Predicted and observed BOLD activity in one example vertex, elicited in response to our bandpass noise stimuli in the deprived eye PRE (pink) and POST deprivation (red), with best fit spatial frequency cut off (reported in the legend).

C-D: Best fit spatial frequency cut-off, averaged in sub-regions of V1 defined by pRF eccentricity bands, and estimated separately for the two eyes and PRE/POST deprivation.

Figure 6: Deprivation effects on the deprived eye population Spatial Frequency Tuning and binocular rivalry phase duration are correlated.

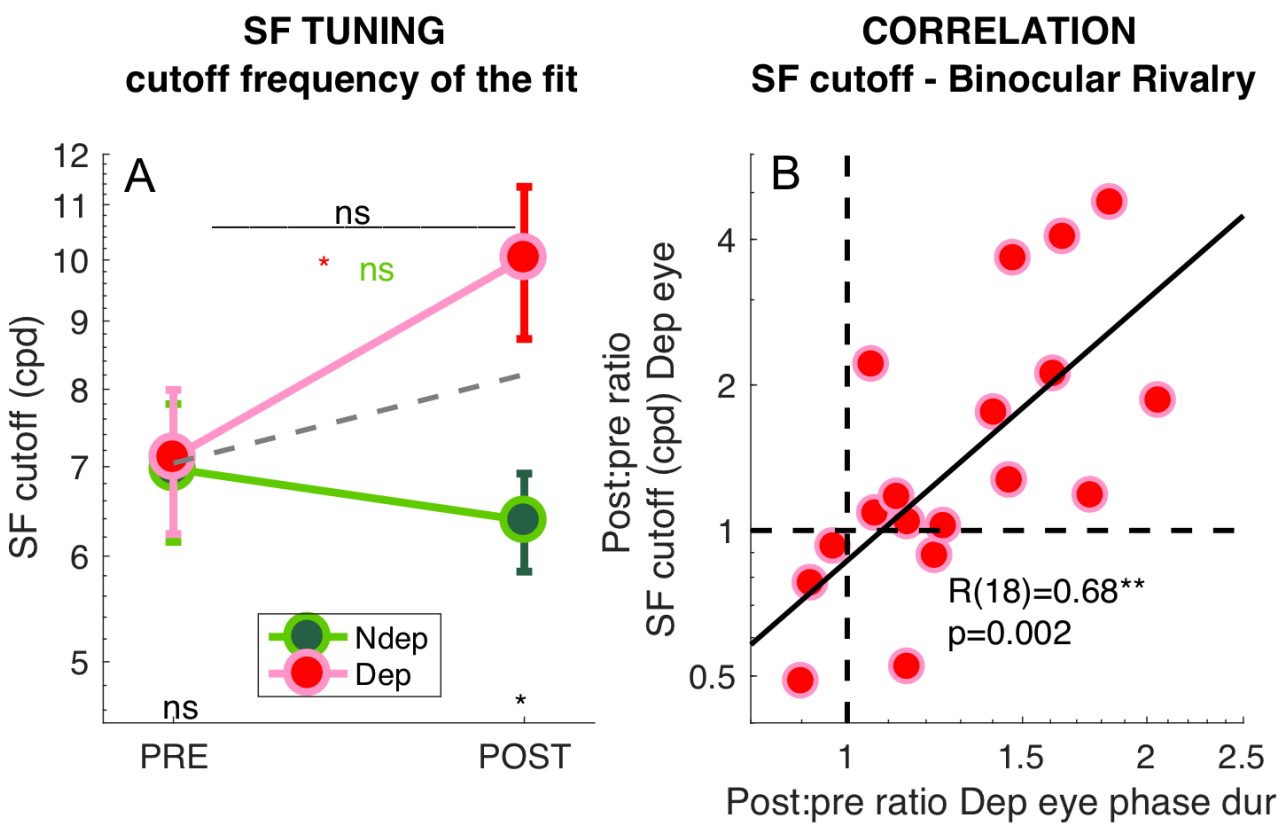


A: Effect of deprivation on spatial frequency cut off values. Average cut-off across all V1 vertices (pooled across eccentricities) for the deprived and non-deprived eye, before and after deprivation, same conventions as in Fig. 1D. Distributions of the log-values do not deviate from normality (Jarque-Bera hypothesis test of composite normality, all $p > 0.285$).

B: Correlation between the POST/PRE ratio (Eq. 7 in the Methods) computed for the binocular rivalry mean phase duration and for the spatial frequency cut off for the deprived eye.